Liver Pathology and SARS-CoV-2 Detection in Formalin-Fixed Tissue of Patients With COVID-19

A Single-Institution Experience

Yevgen Chornenkyy, MD, MSc,[1] Melissa Mejia-Bautista, MD,[1*] Melanie Brucal, MB(ASCP^i),[1] Timothy Blanke, SV(ASCP),[1] David Dittmann, MSc,[1] Anjana Yeldandi, MD,[1] Justin R. Boike, MD, MPH,[2] Jon W. Lomasney, MD, PhD,[1,3] Ritu Nayar, MD,[1] Lawrence J. Jennings, MD, PhD,[1] and Maryam Kherad Pezhouh, MD, MSc[1]*

From the Departments of [1]Pathology, [2]Gastroenterology and Hepatology, and [3]Pharmacology, Northwestern University, Feinberg School of Medicine, Chicago, IL, USA.

Key Words: Autopsy; Gastrointestinal; Hepatopathology; Cytopathology; Molecular diagnostics

Am J Clin Pathol 2021;XX:1–0

DOI: 10.1093/AJCP/AQAB009

ABSTRACT

Objectives: *The novel coronavirus, severe acute respiratory syndrome coronavirus 2, causing coronavirus disease 2019 (COVID-19) remains a global health threat and a significant source of human morbidity and mortality. While the virus primarily induces lung injury, it also has been reported to cause hepatic sequelae.*

Methods: *We aimed to detect the virus in formalin-fixed tissue blocks and document the liver injury patterns in patients with COVID-19 compared with a control group.*

Results: *We were able to detect viral RNA in the bronchioalveolar cell blocks (12/12, 100%) and formalin-fixed, paraffin-embedded tissue of the lung (8/8, 100%) and liver (4/9, 44%) of patients with COVID-19. Although the peak values of the main liver enzymes and bilirubin were higher in the patients with COVID-19 compared with the control group, the differences were not significant. The main histologic findings were minimal to focal mild portal tract chronic inflammation (7/8, 88%, P < .05) and mild focal lobular activity (6/8, 75%, P = .06).*

Conclusions: *We found that most patients who died of COVID-19 had evidence of mild focal hepatitis clinically and histologically; however, the virus was detected in less than half of the cases.*

Key Points

- We detected viral RNA in the bronchioalveolar cell blocks (12/12, 100%) and formalin-fixed, paraffin-embedded tissue of the lung (8/8, 100%) and liver (4/9, 44%) of patients with coronavirus disease 2019 (COVID-19).
- The main histologic findings were minimal to focal mild portal tract chronic inflammation and mild focal lobular activity.
- Most patients who died of COVID-19 had evidence of mild focal hepatitis clinically and histologically; however, the virus was detected in less than half of the cases.

In December 2019, a novel severe acute respiratory syndrome coronavirus 2 (SARS-CoV-2) was identified in Wuhan, China, sparking the global coronavirus disease 2019 (COVID-19) pandemic.[1,2] As of November 25, 2020, according to the COVID-19 Dashboard by the Center of Systems Science and Engineering at Johns Hopkins University, 59,917,575 people worldwide have been diagnosed with COVID-19 and more than 1,412,388 of them have died from its complications.[3]

SARS-CoV-2 is a member of the coronaviruses family, which comprises a diverse group of large, enveloped, nonsegmented, positive-sense single-stranded RNA viruses.[1] SARS-CoV-2 enters human cells by the interaction of the spike (S) protein receptor binding domain with the cell surface receptor protein, angiotensin-converting enzyme 2 (ACE2), leading to the internalization of the complex by the host cell.[4-7] ACE2 protein has ubiquitous distribution and was previously reported in alveolar

epithelial cells, nasal and oral mucosa, small intestine enterocytes, vascular endothelium, bile ducts, and kidney proximal tubular cells.[7] The maximum ACE2 protein expression, according to the consensus data set from the human protein atlas, is found in the small intestine, duodenum, and colon followed by kidney, testis, gallbladder, heart, thyroid gland, adipose tissue, rectum, and lungs.[8] Single-cell RNA sequencing in healthy liver found ACE2 expression is mainly present on cholangiocytes, with 20-fold lower expression in hepatocytes and no expression in Kupffer cells.[9,10] In addition, ACE2 expression is significantly increased in chronic liver disease, which may predispose such patients to worse outcomes.[11]

SARS-CoV-2 induces a systemic disease causing major multiorgan damage, mortality, and sequelae. The lungs are affected the most, and the histopathologic findings have been well documented.[2,12,13] Limited studies have documented the microscopic changes of hepatic tissue in COVID-19, and uncertainty remains regarding liver involvement and the potential for chronic liver disease.[13-18] Hepatic injuries cannot be ignored, as the ACE2 receptor expression on both protein and RNA level has been detected in the hepatobiliary system.[7,9,10] Considering the fact that cholangiocytes express ACE2 in the same manner as the type 2 alveolar cells, it is possible the liver may be a potential target for SARS-CoV-2. Furthermore, ACE2 is also expressed on endothelial cells, such as those found in the portal vasculature.[19] To date, several studies have evaluated hepatic pathology in the context of SARS-CoV-2. The largest study, consisting of 40 patients, found that most patients dying of COVID-19 had clinical evidence of hepatitis while histologic findings revealed macrovesicular steatosis, mild acute hepatitis, and portal inflammation.[16] Zhao et al,[20] in a cohort of 17 patients, reported that the most common microscopic findings were fibrin thrombi, sinusoidal megakaryocytes, microvesicular steatosis, mild portal tract inflammation, and zone 3 hemorrhage/necrosis. In addition to this, a study by Sonzogni et al[15] found that the most common findings included minimal hepatitis and significant vascular alterations. Here, we characterized liver findings in autopsy cases with COVID-19 and investigated whether viral RNA could be detected in the bronchoalveolar lavage (BAL) cell blocks, lung, and liver tissues.

Materials and Methods

Patient Demographics, Autopsy Procedure, and Histologic Examination

Demographic and clinical information were collected on all patients, including age, sex, body mass index (BMI), length of hospital stay, and relevant medical history (hypertension, diabetes mellitus, chronic kidney disease, chronic heart disease, and known or suspected chronic liver disease). Initial and peak laboratory values were also reviewed, including aspartate aminotransferase (AST), alanine aminotransferase (ALT), total bilirubin, and albumin.

Postmortem examinations were done according to the Centers for Disease Control and Prevention (CDC) public guidelines for the collection of specimens. The lungs were infused under gravity via the primary/main bronchi and were allowed to fix for 24 hours in formalin before dissection and sampling. The liver was dissected and sampled fresh. The control group was composed of autopsy liver specimens of patients dying of non-COVID-19 related causes at least 6 months prior to the pandemic with no history of chronic heart disease, vascular disease, or liver disease. Representative tissue samples were fixed in 10% formalin prior to processing and paraffin embedding. Tissue sections were stained with H&E, trichrome stain, and CD34 immunohistochemistry. Histologic criteria for evaluating the liver were adapted as previously described.[15,16,21] While the focus of this study is on the liver, the lung findings were evaluated for previously reported lung pathology and are included in the supplemental material (all supplemental materials can be found at *American Journal of Clinical Pathology* online). This study was approved by Northwestern University Institutional Review Board (STU#00212436). Time to autopsy (TTA), measured in both days and hours, was recorded for COVID-19 and control groups.

Immunohistochemistry

Sections were placed in a 58°C to 60°C oven over 2 hours for tissue to adhere. All dewax and retrieval methods were completed using the Leica Bond Max Autostainer (specifically, protocol F). Slides were dewaxed using Leica Bond Dewax Solution (AR9222). Antigen retrieval was achieved using ER2 (Epitope Retrieval 2 [AR9640] PH9; Leica Biosystems) for 20 minutes. Tissue was blocked with the Bond Polymer Refine Detection Kit (DS9800) for 5 minutes before applying CD34 RTU (QBEnd/10 cat. PA0212; Leica Biosystems) and incubated for 15 minutes. Tissue was blocked again for 8 minutes. DAB Refine was applied and tissue was incubated for 10 minutes. All slides were rehydrated via alcohol/xylene series, mounted, and coverslipped. Appropriate known control tissue (tonsil) was used.

Trichrome Staining

Unstained formalin-fixed paraffin slides were deparaffinized, hydrated, and fixed in Bouin's solution and rinsed. Weigert's solution was applied for 7 minutes. Tissue was washed, dipped in 1% acid alcohol (0.5% HCl

DOI: 10.1093/ajcp/aqab009

in 70% ethanol), washed, and stained in Biebrich scarlet-acid fuchsin for 2 minutes. It was rinsed again, stained in phosphomolydic-phosphotungstic acid solution for 6 minutes, rinsed, stained in aniline blue for 5 minutes, rinsed, dipped in 1% glacial acetic acid, and rinsed. Tissue was dehydrated using alcohol/xylene series and coverslipped using xylene-based mounting medium.

Molecular Detection of Viral RNA in Formalin-Fixed, Paraffin-Embedded Tissue

Testing was performed by using a laboratory-developed version of the CDC SARS-CoV-2 reverse transcription polymerase chain reaction (RT-PCR) assay.[22] The primer/probe sets and control RNAse P primer/probe set are publicly available.[22,23] The assay was applied to formalin-fixed, paraffin-embedded tissue (FFPE) and evaluated with confirmed positive BAL specimens **Table 1**. Briefly, 12 previously confirmed positive BAL specimens were deidentified, randomized, and converted to FFPE cell blocks. Eleven unstained (0.5-µm) slides were cut from each block—one slide to evaluate cellularity by H&E, the remainder for RNA extraction. Cellularity was scored as high cellularity (HC) (>20 cells/10 high-power fields [hpf]; ×40 objective; 0.0030 mm^2) or low cellularity (LC) (<19 cells/×40 objective; 0.0030 mm^2) **Figure 1** and **Table 2**. RNA was extracted using the Covaris truXTRAC FFPE Total NA Plus Kit (cat. 520246) and quantified using the Qubit RNA BR Assay Kit (ThermoFisher; cat. Q10211) (lower limit of detection <5 ng/µL). Reverse transcription was performed by TaqPath 1 StepRT-qPCR MM CG (A15299) (Thermo Fisher Scientific) using the 2019-nCOV Kit (IDT 10006606; Integrated DNA Technologies). PCR was performed on QuantStudio 6 flex (Thermo Fisher Scientific). The reported limit of detection is 500 copies/mL. Cycle threshold values less than 34.5 were considered positive (+), 34.5 to 40 as indeterminate/low positive (+/–), and more than 40 as undetected. Three previously confirmed negative FFPE BAL specimens (high cellularity) and confirmed negative resection tissue were run as negative controls and were negative.

Generation of FFPE BAL Cell Blocks

BAL fluid was centrifuged to form a pellet, supernatant was poured off, and one to three drops of plasma and thrombin were added, mixed, and clotted. Paraffin tissue sections were cut at 0.5 µm thickness, stained with H&E, and examined under light microscopy (Figures 1A-1D).

Data Analysis and Imaging

Continuous demographic variables were expressed as means with ranges. Categorical variables are shown as fraction (percentage). Clinical features among those with and without detectable virus by PCR were compared using Fisher exact test for categorical variables. Continuous nonpatient data were expressed as means and compared by Student *t* test (two tailed). Data analysis was done using GraphPad Prism 8.0 (GraphPad Software). Slide images were captured by Olympus DP73 (Olympus Life Science) and visualized

Table 1
Patient Demographics of COVID-19 Cases and Controls[a]

Patient	Age, y	Sex	BMI, kg/m^2	LoHS	PMHx	pAST, U/L	pALT, U/L	TB	Albumin
C19-1	81	F	24.19	6	DHKL	69	27	0.8	3.1
C19-2	71	M	31.91	1		71	91	2	3.6
C19-3	42	M	41.4	21		5,617	4,926	8.9	4
C19-4	54	M	31.85	29		146	66	6	3.7
C19-5	61	F	39.54	17	DHK	3,510	803	7.8	3.8
C19-6	76	F	18	1	DHK	20	10	0.9	3
C19-7	18	F	42.37	13	DHL	1,470	9,961	44.1	3.2
C19-8	35	F	36.37	52		108	214	1.4	3.8
	57.5 (18-81)	F: 5 (62.5) M: 3 (37.5)	34 (18-42.37)	15 (1-52)	C: 0/8 (0) D: 4/8 (50) H: 4/8 (50) K: 3/8 (37.5) L: 2/8 (25)	146 (20-1,470)	214 (10-9,961)	6.0 (0.8-4.1)	3.7 (3.1-3.8)
C-1	62	M	23.24	0		37	23	0.4	3.2
C-2	37	F	49	2	H	11	12	0.2	4.2
C-3	74	F	35	3	H	615	228	0.5	1.5
C-4	36	F	24	10		15	8	0.9	3.9
	49.5 (36-74)	F: 3 (75) M: 1 (25)	29.5 (23.24-49)	2.5 (0-10)	H: 2/4 (50)	26 (11-615)	17.5 (8-228)	0.45 (0.2-0.9)	3.55 (1.5-4.2)

BMI, body mass index; C, cardiac; D, diabetes; H, hypertension; K, chronic kidney disease; L, chronic liver disease; LoHS, length of hospital stay; pALT, peak alanine transaminase; pAST, peak aspartate transaminase; PMHx, past medical history; TB, total bilirubin.
[a]Patient's age, sex, BMI, medical history, and selected laboratory values. Results are presented as mean (range) or number (%).

DOI: 10.1093/ajcp/aqab009

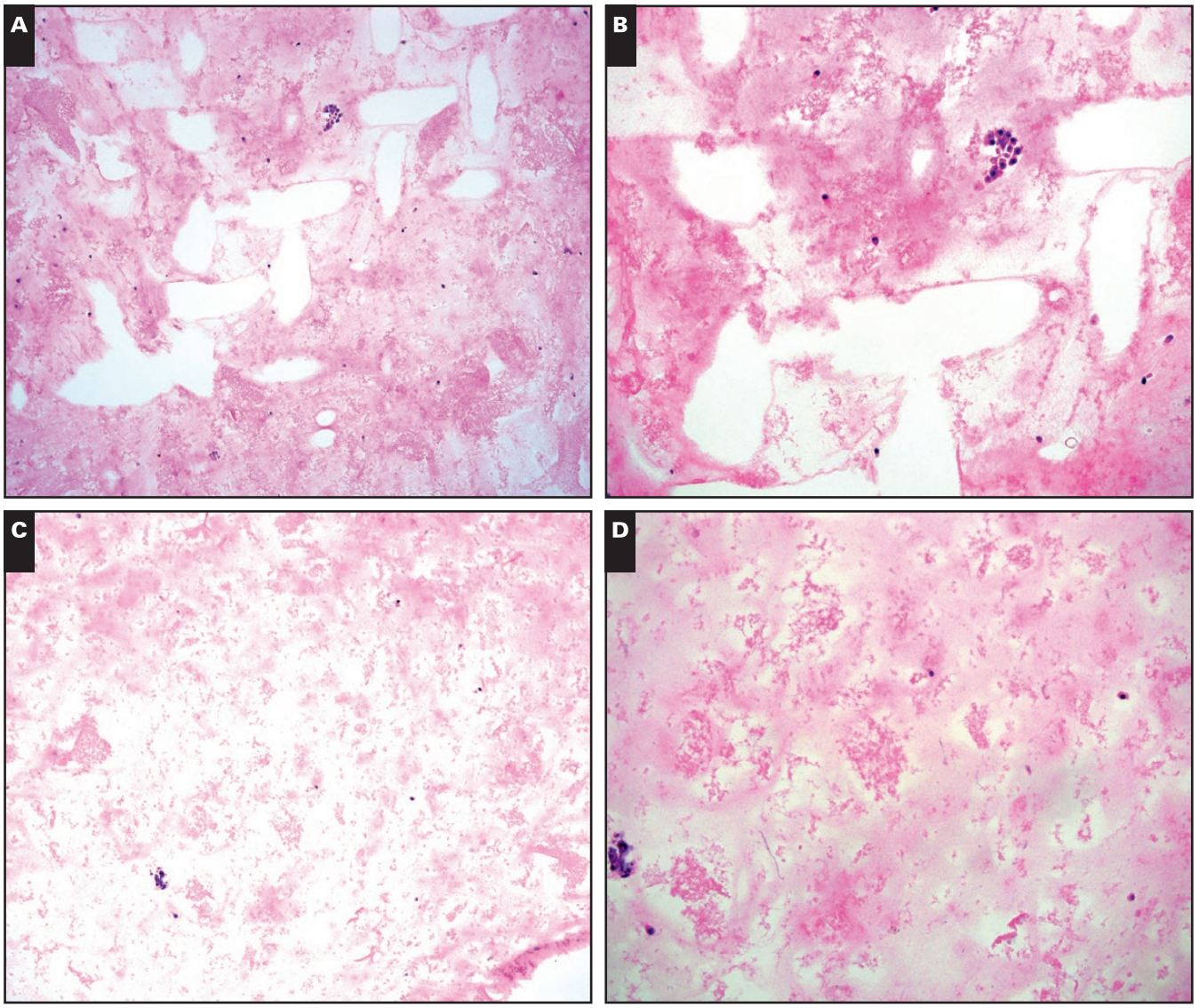

Figure 1 Detection of viral RNA in bronchoalveolar lavage (BAL) cell blocks. **A**, **B**, An example of a high-cellularity (HL) cell block (COVID 5 + BAL). **C**, **D**, An example of a low-cellularity (LC) cell block (COVID 6 + BAL).

by CellSens Standard v.1.9 (Olympus Life Sciences) on a Windows operating system (Intel, Core i7-4770 CPU @ 3.40 GHz).

Results

Patient Demographics and Laboratory Values

A total of nine cases with COVID-19 (group C19) were initially included in our study, but one case (case 9) contained significant autolysis precluding histologic evaluation and was excluded from the cohort when evaluating histology and clinical laboratory parameters (n = 8) (Table 1). Despite significant tissue autolysis, viral RNA in lung tissue was detected, and case 9 was included only in Figure 2. Of the remaining eight cases that had adequate tissue for histologic analysis, five (62.5%) were female and three (37.5%) were male. The median age was 57.5 years (range, 18-81 years), and six (75%) were overweight (BMI >30 kg/m^2). The diagnosis of COVID-19 in all cases was made by nasopharyngeal swab molecular tests. The median hospital stay was 15.5 days (range, 1-52 days). Most patients had a medical history of hypertension (4/8, 50%) and/or diabetes mellitus (4/8, 55%). Two (22%) patients had a history of chronic liver disease, one with hepatitis C viral infection (HCV) and one with a history autoimmune hepatitis following orthotopic liver transplant with multiple episodes of rejections. The patients had a broad spectrum of symptoms, including fevers, poor appetite, diarrhea, abdominal pain, shortness

DOI: 10.1093/ajcp/aqab009

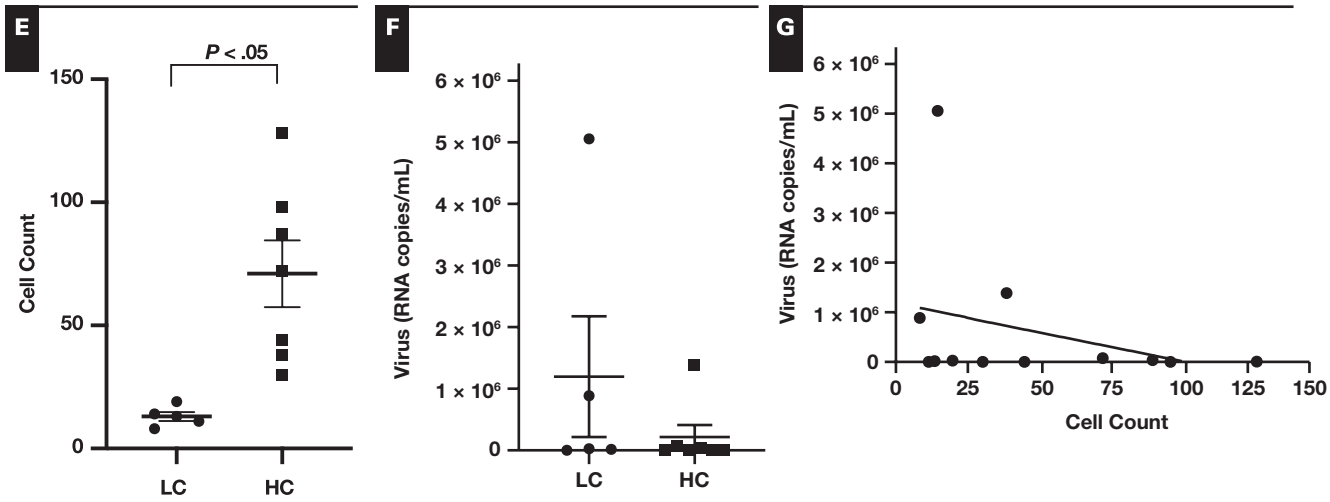

Figure 1 (cont) **E**, Comparison cell counts in LC- and HC-designated cell blocks. **F**, Virus RNA copies per mL in LC and HC cell blocks. **G**, Linear regression analysis of cell count to virus RNA copies per mL. *$P < .05$. Error bars, SEM. (H&E; **A**, **C**, ×100; **B**, **D**, ×200)

Table 2
Detection of Viral RNA in Bronchoalveolar Lavage (BAL) Cell Blocks

Sample Name	N1 Cycle Threshold[a]	Virus, copies/mL	Cellularity[b]	Cell Count[c]	RNA, ng/μL[d]
COVID 1 + BAL	27.517	25,562	Low	19	<5
COVID 2 + BAL	31.245	1,751	Low	11	<5
COVID 3 + BAL	30.579	2,827	High	44	<5
COVID 4 + BAL	31.812	1,165	High	30	<5
COVID 5 + BAL	25.962	78,192	High	72	<5
COVID 6 + BAL	20.163	5,057,633	Low	14	<5
COVID 7 + BAL	22.584	887,097	Low	8	<5
COVID 8 + BAL	21.96	1,389,377	High	38	<5
COVID 9 + BAL	28.879	9,600	High	128	<5
COVID 10 + BAL	28.024	17,753	Low	13	<5
COVID 11 + BAL	27.031	36,254	High	87	<5
COVID 12 + BAL	32.356	788	High	93	<5

[a]Positive, <34.5; indeterminate/low positive, 34.5-40; undetected, >40.
[b]Low, <19; high, ≥20.
[c]Cell count was determined by counting ten 40x fields.
[d]Approximate RNA copies per μL is given based on standard controls.

of breath, confusion, headache, dry cough, and myalgias. Patient characteristics and known comorbidities are summarized in Table 1. Our control group (C) was composed of four patients who died of nonliver, noncardiac, and nonpulmonary etiologies for comparison of laboratory and histologic findings. While C19 peak AST, ALT, and total bilirubin were increased on average relative to the C group, the differences were not significant. The mean time from dying to autopsy was not significantly different between C19 and C groups (Figure 2C).

Viral PCR

At the time this study was undertaken, the standard PCR for the COVID-19 assay in FFPE tissue was not available, and instead the SARS-COV-2 primer/probe sets per CDC recommendations designed for detecting virus in BAL specimens were used. Formalin fixation is known to degrade RNA to an average size range of 100 to 270 nucleotides (nt).[24] However, amplicons containing fewer than 200 nt, specifically 158 base pairs (bp), were reported to be amplified 96% of the time, whereas amplicons of 374 bp were not consistently detected.[24] The expected amplicon size for N1 was 72 bp, and RNaseP was 65 bp using CDC primer/probe sets. The RT-PCR was first evaluated on 12 random deidentified previously known positive BAL samples that were converted to FFPE cell blocks and four negative controls **Figure 1A**, **Figure 1B**, **Figure 1C**, and **Figure 1D**. All tested BAL cell blocks from patients with COVID-19 were positive (12/12, 100%) (Table 2). Moreover, all the BAL

DOI: 10.1093/ajcp/aqab009

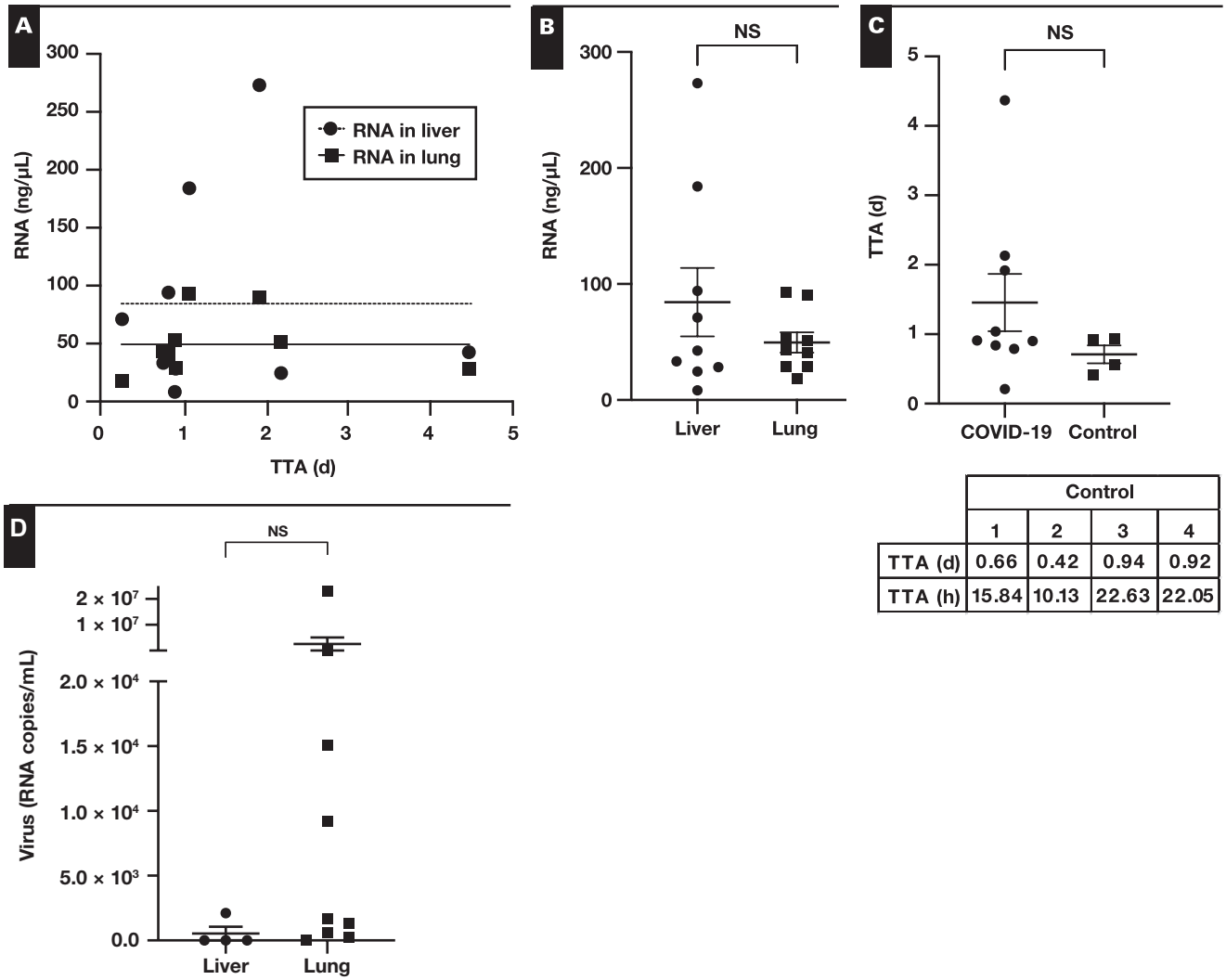

	Control			
	1	2	3	4
TTA (d)	0.66	0.42	0.94	0.92
TTA (h)	15.84	10.13	22.63	22.05

Figure 2 Detection of viral RNA liver and lung formalin-fixed, paraffin-embedded tissue. **A**, Linear regression analysis of total RNA concentration in lung and liver tissues relative to time to autopsy (TTA) in days. **B**, Comparison of average total RNA extracted from liver and lung autopsy tissues. **C**, Comparison of TTA in days between coronavirus disease 2019 (COVID-19)–positive autopsies and COVID-19–negative autopsies (controls). **D**, Comparison of average of total virus copies per mL extracted from liver and lung autopsy tissues. Error bars, SEM.

Table 3

Detection of Viral RNA Liver and Lung Formalin Fixed Paraffin Embedded Tissue in Autopsy Lungs and Livers

Patient	Time to Autopsy, d (h)	Liver	N1 Cycle Threshold[a]	Virus, copies/mL	RNA, ng/µL	Lung	N1 Cycle Threshold[a]	Virus, copies/mL	RNA, ng/µL
1	0.21 (5.04)	+/–	37.732	16	71	+	18.054	23,040,871	18.054
2	1.04 (24.96)	+/–	37.795	15	184	+	28.938	9,202	93
3	2.13 (51.12)	+/–	37.282	22	24.6	+	31.647	1,312	51
4	1.92 (46.08)	–	UND	NA	279	+	34.168	214	90
5	0.91 (21.84)	–	UND	NA	28.4	+	28.249	15,101	29
6	0.84 (20.16)	–	UND	NA	94	+	24.424	236,274	41.2
7b		–	UND	NA	22				
7a	0.90 (21.6)	+	30.99	2,104	8.33	+	31.325	1,653	53
8	0.79 (18.96)	–	UND	NA	33.3	+/–	37.197	24	43.2
9	4.37 (104.88)	–	UND	NA	42.6	+	32.725	604	28.5

[a]Positive, <34.5; indeterminate/low positive, 34.5-40; undetected, >40.

DOI: 10.1093/ajcp/aqab009

Table 4
Stratification of Liver Pathology Findings in COVID-19 Relative to PCR Status[a]

Pathologic Features	PCR Positive (n = 4)	PCR Negative (n = 4)	*P* Value[b]
Portal vein dilatation or phlebosclerosis	0 (0)	0 (0)	
Vascular herniation	0 (0)	0 (0)	
Periportal abnormal vessels	0 (0)	0 (0)	
Vascular thrombosis	0 (0)	0 (0)	
Fibrosis (Batts-Ludwig grade)			.99
Absent	3/4 (75)	2/4 (50)	
Periportal fibrous expansion (mild fibrosis)	0 (0)	2 (50)	
Portoportal septa (moderate fibrosis)	0 (0)	0 (0)	
Portocentral septa (severe fibrosis)	1 (25)	0 (0)	
Necrosis			.99
Absent (necrosis)	2/4 (50)	2/4 (50)	
Focal (<25%)	0 (0)	0 (0)	
Multifocal (26%-74%)	1 (25)	1 (25)	
Diffuse (>75%)	1 (25)	1 (25)	
Location (zones 1, 2, 3)	2 and 3	2, 2, and 3	
Lobular parenchymal activity			.4286
Absent (grade 0)	0/4 (0)	2/4 (50)	
Minimal, inflammation without necrosis (grade 1)	3 (75)	2 (50)	
Mild, focal hepatocellular necrosis (apoptotic bodies) with inflammation (grade 2)	0 (0)	0 (0)	
Moderate, focal hepatocellular damage with necrosis (grade 3)	0 (0)	0 (0)	
Severe, hepatocellular damage with portoportal/ portocentral bridging necrosis (grade 4)	1 (25)	0 (0)	
Portal inflammation			.99
Absent (0)	0/4 (0)	1/4 (25)	
Focal (<25%)	2 (50)	3 (75)	
Multifocal (26%-74%)	0/4 (0)	0/4 (0)	
Diffuse (>75%)	2/4 (50)	0 (0)	
Type, case number	1,2-L,PC; 3-L; 8-L,PC,rE	5,-L,PC; 6-L,N;9-L	
Bile ducts			
Unremarkable	2/4 (50)	2/4 (50)	.99
Bile plugs	0/4 (0)	1/4 (25)	
Reactive/proliferative	2/4 (50)	1/4 (25)	
Congestion			.99
Absent	1/4 (25)	0/4 (0)	
Present	3/4 (75)	4 (100)	
Steatosis			.99
Absent	2/4 (50)	2/4 (50)	
Microvesicular	0/4 (0)	0/4 (0)	
Macrovesicular	2 (25) mild (5-33)	1 (25) mild (5-33), 1 (25) moderate (34-75)	
Additional findings	None	1/4 (25)—hemosiderin deposition	
CD34			.99
Unremarkable	3/4 (75)	4/4 (100)	
Increased relative to controls	1/4 (25)	0 (0)	
Masson Trichrome			.99
Unremarkable	3/4 (75)	2/4 (50)	
Increased	Case 1—stage IV fibrosis	Cases 6 and 7—mild expansion of portal areas	

COVID-19, coronavirus disease 2019; L, lymphocytes; n, neutrophils; PC, plasma cells; PCR, polymerase chain reaction; rE, rare eosinophils.
[a]Values are presented as number (%) unless otherwise indicated.
[b]Fisher exact test.

cell blocks of patients negative for COVID-19 were negative (not shown). While based on cell counts, the cell blocks could be stratified based on HC (≥20 cells/10 hpf) and LC (<20 cells/10 hpf) ($P < .05$) (Figure 1E), the relationship between cell block cellularity and viral RNA concertation extracted was nonsignificant ($P = .22$) **Figure 1F** and **Figure 1G**. Interestingly, the virus was detected in cell blocks with as little as eight cells/10 hpf (Table 1).

The RT-PCR performed on nine autopsy lungs and livers was positive in all lung specimens (9/9, 100%) but positive in only four liver specimens (4/9, 44%) **Table 3**. TTA ranged from 0.21 to 4.37 days (mean, 1.46 days in

DOI: 10.1093/ajcp/aqab009

Table 5
Summary of Hepatic Pathologic Features in COVID-19 Cases and Non–COVID-19 Controls[a]

Pathologic Features	COVID-19 (n = 8)	Controls (n = 4)	*P* Value[b]
Portal vein dilatation or phlebosclerosis	0 (0)	0 (0)	
Vascular herniation	0 (0)	1/4 (<25% of vessels)	
Periportal abnormal vessels	0 (0)	0 (0)	
Vascular thrombosis	0 (0)	0 (0)	
Fibrosis (Batts-Ludwig grade)			.4909
Absent	5/8 (63)	4/4 (100)	
Periportal fibrous expansion (mild fibrosis)	2 (25)		
Portoportal septa (moderate fibrosis)	0 (0)		
Portocentral septa (severe fibrosis)	1 (12)		
Necrosis			.2081
Absent (necrosis)	4/8 (50)	4/4 (100)	
Focal (<25%)	0 (0)		
Multifocal (26%-74%)	2 (25)		
Diffuse (>75%)	2 (25)		
Location (zones 1, 2, 3)	2 and 3		
Lobular parenchymal activity			.0606
Absent (grade 0)	2/8 (25)	4/4 (100)	
Minimal, inflammation without necrosis (grade 1)	5 (63)		
Mild, focal hepatocellular necrosis (apoptotic bodies) with inflammation (grade 2)	0 (0)		
Moderate, focal hepatocellular damage with necrosis (grade 3)	0 (0)		
Severe, hepatocellular damage with portoportal/portocentral bridging necrosis (grade 4)	1 (12)		
Portal inflammation			.0101
Absent	1/8 (12)	4/4 (100)	
Focal (<25%)	5 (63)		
Multifocal (26%-74%)	0 (0)		
Diffuse (>75%)	2 (25)		
Type	1,2,5,-L,PC;3-L;6-L,N; 8-L,PC,rE; 9-L		
Bile duct changes			.2081
Unremarkable	4/8 (50)	4/4 (100)	
Bile plugs	1/8 (12)		
Reactive/proliferative	3/8 (38)		
Congestion			.5475
Absent	2/8 (25)	2/4 (50)	
Present	6 (67)	2 (50)	
Steatosis			.5758
Absent	4/8 (50)	3/4 (75)	
Microvesicular	0 (0)	0 (0)	
Macrovesicular	3 (12) mild (5-33); 1 (12) moderate (34-75)	1 (25) mild (5-33)	
Additional findings	1/8 (12)—hemosiderin deposition	None	
CD34			.99
Unremarkable	7/8 (88)	4/4 (100)	
Increased relative to controls	1/8 (12)	NA	
Masson Trichrome			.4909
Unremarkable	5/8 (63)	4/4 (100)	
Increased	Case 1—stage IV fibrosis; cases 6 and 7—mild expansion of portal areas	NA	

COVID-19, coronavirus disease 2019; NA, not applicable.
[a]Values are presented as number (%) unless otherwise indicated.
[b]Fisher exact test.

COVID-19 cohort vs 0.735 days in control cohort), and there was no significant relationship between TTA and amount of RNA extracted from tissues (Figures 2A-2C). In the BAL cell blocks, the viral copies per milliliter (cp/mL) ranged from 788 to 5,057,633. The viral copies ranged from 24 to 23,040,871 cp/mL in the lungs and 16-2,104 cp/mL in the liver. While the average viral copies in the lung were higher than the liver (2,589,473 vs 539 cp/mL), this difference was not statistically significant ($P = .52$). Interestingly, one case in which the liver was biopsied prior to undergoing autopsy was negative for viral particles on the biopsy specimen prior to death and positive at the time of autopsy (Table 3, cases 7b and 7a). In our cohort, there were no significant correlations between liver PCR

DOI: 10.1093/ajcp/aqab009

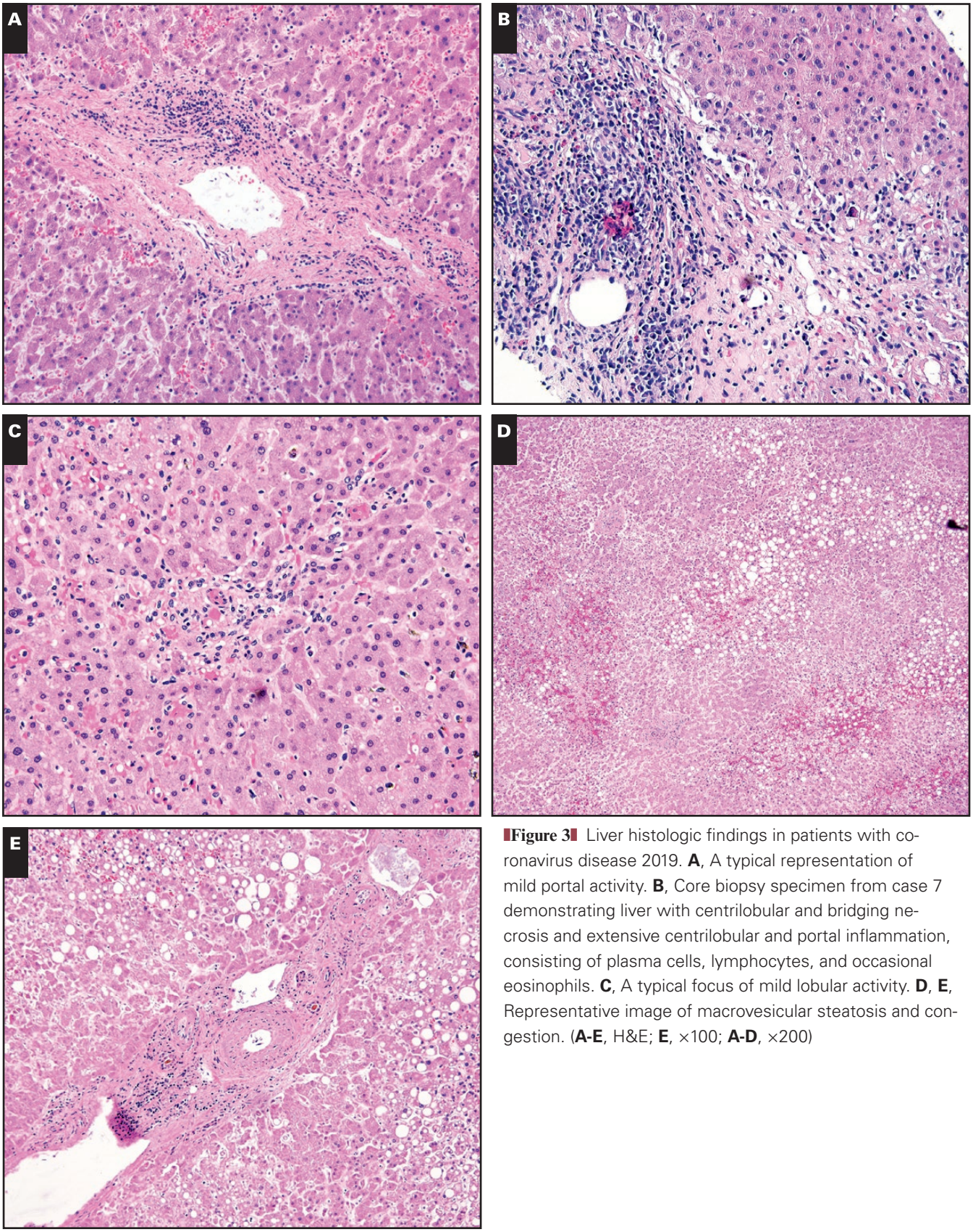

Figure 3 Liver histologic findings in patients with coronavirus disease 2019. **A**, A typical representation of mild portal activity. **B**, Core biopsy specimen from case 7 demonstrating liver with centrilobular and bridging necrosis and extensive centrilobular and portal inflammation, consisting of plasma cells, lymphocytes, and occasional eosinophils. **C**, A typical focus of mild lobular activity. **D**, **E**, Representative image of macrovesicular steatosis and congestion. (**A-E**, H&E; **E**, ×100; **A-D**, ×200)

DOI: 10.1093/ajcp/aqab009

positivity and histologic findings **Table 4**. Interestingly, we detected viral particles in case 9 at 4.37 days (104.88 hours) after the patient died, despite extreme tissue autolysis precluding histologic analysis.

Histopathologic Findings

The lungs were evaluated microscopically to confirm the presence of previously reported pulmonary findings.[12] Diffuse alveolar damage was observed in six (75%) of eight cases, and additional findings are documented in the supplement (Supplementary Figure 1). Livers, on gross examination, showed varying degrees of yellow discoloration and congestion. A summary of observed pathologic liver findings in C19 and C groups is provided in **Table 5**, **Figure 3**, and Supplementary Figure 2. Microscopically, the livers of C19-positive cases showed significant mild focal portal chronic inflammation relative to controls (7/8, 88%, P = .01; Figure 3A). Additional findings that did not reach significance were mild focal lobular activity (6/8, 75%, P = .06; Figure 3C); mild congestion (6/8, 75%, P = .054; Figures 3D and 3E); macrovesicular steatosis (4/8, 50%, P = .57; Figures 3D and 3E); bile duct changes (P = .20), including bile plugs (1/8, 12%), bile ductular proliferation (4/8, 50%), and necrosis (4/8, 50%, P = .2; Figure 3B); and fibrosis (3/8, 38%, P = .49). Relative to the C group, mild focal portal activity was significantly increased in the C19 group (P = .01), while mild lobular activity approached significance (P = .06). None of our C19 group showed central vein herniation, but one case in the control group showed rare focal central vein herniation (Supplementary Figures 2D and 2E). In the C19 group, the case with focal bile plugs had a history of sepsis, while the two cases with increased bile duct proliferation had histories significant for HCV infection and autoimmune hepatitis following liver transplant. Stratification of liver findings between C19 PCR positive and C19 PCR negative did not reveal significant differences or notable trends.

Portal Activity

Seven cases of the C19 group (7/8, 63%) had portal inflammation that was significantly increased relative to our C group (P = .01). The portal inflammation was mild, focal (present in <25% of portal tracts), and composed of lymphocytes (Figure 3A). Two cases had diffuse inflammation (present in >75% of portal tracts), one of which had a history of HCV infection, and contained generally mild but diffuse lymphocytic portal inflammation. The other case had a history of autoimmune hepatitis following liver transplant with multiple episodes of T-cell–mediated rejection and contained significant diffuse portal inflammation that was more prominent on the biopsy specimen prior to death compared with the autopsy liver (Figure 3B).

Parenchymal Activity (Acute Hepatitis)

Six (75%) of eight cases contained mild focal lobular activity (acute hepatitis) that was approaching significance relative to the control group (P = .06). In five cases, the activity was minimal without necrosis (Figure 3C). Although rare apoptotic bodies were seen in some cases, this finding was not prominent in our series. One case in our series had a history of autoimmune hepatitis following orthotopic liver transplant with multiple episodes of T-cell–mediated rejection (acute cellular rejection). Core biopsy specimen (Figure 3B) prior to death demonstrated extensive portal inflammation, consisting of plasma cells, lymphocytes, and occasional eosinophils, along with bile ductulitis and endothelialitis as well as centrilobular and bridging necrosis. These findings were favored to be related to severe plasma cell rich rejection. Microscopic examination of liver after autopsy demonstrated similar findings.

Steatosis and Sinusoidal Capillarization

Macrovesicular steatosis was present in four (50%) of eight cases, and relative to our control cohort (1/4, 25%), this was not significant (P = .57) (Figures 3D and 3E). Overall, the macrovesicular steatosis was typically mild (3/4, 75%) in most cases and moderate in one case (1/4, 25%). Sinusoidal capillarization was evaluated by CD34 immunostaining and compared between the groups. Overall, aberrant sinusoidal capillarization was not observed.

Additional Findings

Less frequently observed findings were necrosis (4/8, 50%) and fibrosis (3/8, 38%). Two of these cases showed multifocal necrosis (26%-74% of liver parenchyma) and two cases with diffuse necrosis (>75%). One of the cases with multifocal necrosis had no medical history but during hospitalization developed *Clostridium difficile* colitis, leading to ischemic colon. The second case had a history significant for end-stage renal disease and type 2 diabetes and during hospitalization developed septic shock secondary to *Klebsiella pneumoniae* and SARS-CoV2 complicated by *C difficile* colitis and transmural bowel necrosis. Of the two cases with diffuse necrosis, one had a history of autoimmune hepatitis following transplant with multiple episodes of rejections (Figure 3B), whereas the second one had a history of systemic lupus erythematosus and developed septic shock and acute respiratory distress syndrome

DOI: 10.1093/ajcp/aqab009

secondary to SARS-CoV-2. Fibrosis was observed in three cases, two of which contained mild focal fibrosis consisting of mild periportal fibrous expansion and one case with cirrhosis with a history of HCV infection. In addition, one case showed increased hemosiderin deposition in Kupffer cells and sinusoids. The patient's clinical history was limited but significant for end-stage renal disease. Overall, we attribute the necrosis to other contributing factors rather than COVID-19–related changes.

Discussion

Here we present the hepatic findings of eight autopsies of patients who died of complications of COVID-19 and compare them with a control group. The main COVID-19–related histologic findings of the livers compared with the control group were mild focal portal activity (7/8, 88%, $P = .01$) and mild lobular activity (6/8, 75%, $P = .06$). In patients who died of COVID-19, the virus was detected in the lungs of all patients (100%), while only 44% of patients in our cohort had the virus in their livers. The average viral copies in the lung were higher than in the liver (2,589,473 vs 539 cp/mL), but this difference was not statistically significant ($P = .52$). Two unexpected findings were detection of virus in all BAL cell blocks, including ones with as little as eight cells per 10 hpf, and the second was detection of viral particles in the lungs of a patient who died 4.37 days (104.88 hours) prior, despite tissue autolysis precluding adequate histologic read. This raises the question of how long the viral particles can persist in the tissue postmortem and whether those tissues can be a source of infection.

Mild focal portal tract chronic inflammation was commonly seen (n = 7/8, 88%, $P = .01$) and was significantly increased relative to the control cases, but the portal tract inflammation was mild and focal. These findings are similar to what was recently reported in a series of 40 autopsies.[16] In their cohort, 20 (50%) cases contained portal inflammation, 3 contained interface hepatitis, and the remainder (17 cases) contained minimal increased portal mononuclear cells composed of lymphocytes and few portal macrophages.[16] Similarly, a series of 12 autopsies in Europe described minimal lymphoplasmacellular portal infiltrate.[25] Two of our cases contained diffuse portal tract inflammation, but these findings can be linked to their underlying medical conditions. One case with mild diffuse activity had a history of HCV infection and cirrhosis, while the other had an aforementioned history of autoimmune hepatitis. On the biopsy specimen prior to death, the portal infiltrate was composed of lymphocytes, plasma cells, and rare eosinophils, while on autopsy, the portal tract inflammation consisted mostly of lymphocytes with rare plasma cells. It has been previously reported that the ACE2 receptor is present on cholangiocytes, but we did not observe any evidence of bile duct injury.[7] Most of our C19 cases contained mild sinusoidal congestion (6/8, 75%), but this finding was also present in 50% of our C group. Thus, presence of congestion is likely a nonspecific change, and its significance is uncertain.

Mild liver parenchymal activity, without necroinflammation, was present in 63% (5/8, $P = .06$) of our cases, and while it trended toward significance, it was not significantly different compared with our C group. In our series, we did not see frequent single-cell hepatocyte necrosis associated with inflammation. The degree of inflammation was overall mild and focal. In most cases, the mild inflammatory foci were composed of lymphocytes. In the case with aforementioned autoimmune hepatitis, the core biopsy specimen demonstrated portal tract inflammation mainly consisting of rare plasma cells, lymphocytes, and eosinophils, along with bile ductulitis and endothelialitis and centrilobular and bridging necrosis. Overall, the findings were most consistent with severe acute cellular rejection, and the patient was treated with intravenous steroids, sirolimus, and tacrolimus and antithymocyte globulin. The liver autopsy sections demonstrated similar findings, including lobular inflammation, zone 2 and 3 necrosis, and portal inflammation consisting of mostly lymphocytes and rare plasma cells. In this case, we suspect the histologic liver findings are more attributed to rejection and may have been further complicated by COVID-19. While stratification of parenchymal activity by PCR status was nonsignificant ($P = .43$), all patients (4/4) with positive PCR showed mild lobular activity while only 50% (2/4) of negative PCR cases had lobular activity ($P = .08$). Our histologic and PCR stratification findings are similar to those reported in a larger cohort demonstrating mild acute hepatitis in 64% of their PCR-positive cases.[16]

While macrovesicular steatosis was a common finding and present in 50% of C19 cases, it was also detected in one (25%) of four cases in our control group and was not significantly different. Our findings of macrovesicular steatosis are lower than the previously reported findings in the literature. A study performed by a group associated with the CDC found steatosis in 50% of autopsy livers; however, steatosis type was not specified but appears to be macrovesicular.[26] Another study recently reported macrovesicular steatosis in 75% of their patients.[16] In our COVID-19 cohort, the average BMI was 34 kg/m^2, and patients with macrovesicular steatosis had a BMI of 24.2 kg/m^2 and 39.54 kg/m^2 and were diabetic. Features of steatohepatitis were absent. We attribute the steatosis to their underlying comorbidities, with predominantly metabolic etiologies.

The role of endothelial injury in COVID-19 is uncertain. SARS-CoV-2 virus has been demonstrated to

DOI: 10.1093/ajcp/aqab009

be present in endothelial cells, and hepatic lymphocytic endothelialitis has been previously reported.[7,19] In our cohort, histologic vascular abnormalities were not identified; this is similar to a previously reported study[16] and is in contrast to a case series from Italy describing vascular pathology.[15] Furthermore, in contrast to Zhao et al,[20] we did not observe fibrin thrombi in our cohort. To better evaluate vascular findings, we used the CD34 immunostain, a marker highlighting endothelial cells and sinusoidal capillarization. No capillarization was observed in both our COVID-19 cohort and the control group. While one case with cirrhosis secondary to HCV infection had increased portal vascular structures highlighted by CD34 immunostain and very minor sinusoidal capillarization, widespread extensive sinusoidal capillarization was absent. The absence of sinusoidal capillarization could be explained by the fact that sinusoidal capillarization often can be observed only during initial stages of fibrosis.[27]

This study is interesting and important for several reasons. Despite our small cohort, we were able to observe similar findings to recently published studies.[16,25] To ensure that our PCR would be applicable to FFPE samples, we demonstrated that virus can be detected in BAL cell blocks from previously confirmed positive patients, including low-cellularity cell blocks with as little as eight cells per 10 hpf. This finding opens the opportunity to study BAL samples and cytopathology in COVID-19 cases. We were able to demonstrate that all the patients who died of COVID-19 had the virus in the lung tissue, but slightly less than half (45%) contained the virus in the liver. This finding is similar to a recently reported larger cohort demonstrating that slightly more than half of their patients had detectable virus in their liver.[16] Liver PCR positivity in our cohort was not significantly associated with laboratory and histologic findings, but our cohort consisted of eight cases, and thus we were likely underpowered to detect certain associations.

An interesting and somewhat unexpected finding in our cohort is that of a case that underwent a liver biopsy prior to death. The PCR for COVID-19 was negative in the liver biopsy specimen prior to death, but the autopsy liver was found to contain the virus by PCR. The patient had a history of liver transplant with multiple episodes of rejections. This patient was treated with multiple immunosuppressants, including intravenous steroids, sirolimus, tacrolimus, and antithymocyte globulin. It has been previously reported that time between initial diagnosis and death is not a factor associated with liver PCR positivity.[16] While we are cautious, we believe that our PCR result reflects a true positive, as we were able to detect the viral RNA in BAL cell blocks with as little as eight cells and also 4.37 days (104.88 hours) after dying. This indicates that the liver core biopsy done prior to the patient's death was indeed negative at the time of biopsy. This phenomenon may point to an infection time course or a role for immunosuppressants in modulating the effect of COVID-19 on the liver. Previous findings of moderate acute hepatitis in liver allograft recipients have also been reported and demonstrated increased apoptotic hepatocytes and abundant lymphohistiocytic inflammation.[17,18] The effect of immunosuppression and transplant status on liver injury in the context of COVID-19 needs further exploration.

Weaknesses of our study include an autopsy study and limited sample size. To somewhat mitigate this, we included four autopsy cases as a control group and added CD34 immunostaining. All of our control cases were negative for hepatic pathology at death and used to exclude nonspecific findings inherent to autopsy tissue processing (eg, congestion). Furthermore, all of our patients had severe disease leading to demise. It will be important to study liver injury in the context of nonlethal COVID-19. In our cohort, SARS-CoV-2 seems to involve the liver and is associated with mild portal and parenchymal inflammation. We realize that secondary to our sample size, we were underpowered to detect certain associations, and this is quite likely why some of our findings were nonsignificant (eg, average viral copies in the lung vs liver, levels of AST and ALT in COVID-19 vs controls).

Despite our limited cohort, we provided a description of histologic and clinical findings along with detection of the virus in patients dying of complications of COVID-19. We demonstrated that patients dying of COVID-19 complications have abnormal liver enzymes, mild parenchymal and portal activity, and viral RNA in the lungs and liver. In addition, we were able to demonstrate that virus RNA can be detected in BAL cell blocks, lung, and liver tissues of patients with COVID-19. While further studies are needed to evaluate the effect of COVID-19 on the liver, our data, in addition to other studies, point to some liver involvement.

Corresponding author: Maryam K. Pezhouh, MD, MSc; maryam.pezhouh@northwestern.edu.

Acknowledgments: This research was supported by an institutional grant from the Northwestern University Department of Pathology Resident Research Committee.

**First authors.*

References

1. Zhu N, Zhang D, Wang W, et al; China Novel Coronavirus Investigating and Research Team. A novel coronavirus from patients with pneumonia in China, 2019. *N Engl J Med.* 2020;382:727-733.

DOI: 10.1093/ajcp/aqab009

2. Pawlotsky JM. COVID-19 and the liver-related deaths to come. *Nat Rev Gastroenterol Hepatol.* 2020;17:523-525.
3. COVID-19 Dashboard by the Center for Systems Science and Engineering (CSSE) at Johns Hopkins University (JHU). 2020. https://coronavirus.jhu.edu/map.html. Accessed November 25, 2020.
4. Li F, Li W, Farzan M, et al. Structure of SARS coronavirus spike receptor-binding domain complexed with receptor. *Science.* 2005;309:1864-1868.
5. Zhang H, Penninger JM, Li Y, et al. Angiotensin-converting enzyme 2 (ACE2) as a SARS-CoV-2 receptor: molecular mechanisms and potential therapeutic target. *Intensive Care Med.* 2020;46:586-590.
6. Hoffmann M, Kleine-Weber H, Schroeder S, et al. SARS-CoV-2 cell entry depends on ACE2 and TMPRSS2 and is blocked by a clinically proven protease inhibitor. *Cell.* 2020;181:271-280.e8.
7. Hamming I, Timens W, Bulthuis ML, et al. Tissue distribution of ACE2 protein, the functional receptor for SARS coronavirus: a first step in understanding SARS pathogenesis. *J Pathol.* 2004;203:631-637.
8. The Human Protein Atlas. Tissue expression of ACE2. 2020. https://www.proteinatlas.org/ENSG00000130234-ACE2/tissue. Accessed June 28, 2020.
9. Qi F, Qian S, Zhang S, et al. Single cell RNA sequencing of 13 human tissues identify cell types and receptors of human coronaviruses. *Biochem Biophys Res Commun.* 2020;526:135-140.
10. Chai X, Hu L, Zhang Y, et al. Specific ACE2 expression in cholangiocytes may cause liver damage after 2019-nCoV infection. *bioRxiv.* 2020. https://doi.org/10.1101/2020.02.03.931766.
11. Paizis G, Tikellis C, Cooper ME, et al. Chronic liver injury in rats and humans upregulates the novel enzyme angiotensin converting enzyme 2. *Gut.* 2005;54:1790-1796.
12. Vasquez-Bonilla WO, Orozco R, Argueta V, et al. A review of the main histopathological findings in coronavirus disease 2019. *Hum Pathol.* 2020;105:74-83.
13. Tian S, Xiong Y, Liu H, et al. Pathological study of the 2019 novel coronavirus disease (COVID-19) through postmortem core biopsies [published online April 14, 2020]. *Mod Pathol.*
14. Yao XH, Li TY, He ZC, et al. A pathological report of three COVID-19 cases by minimal invasive autopsies. *Zhonghua Bing Li Xue Za Zhi.* 2020;49:411-417.
15. Sonzogni A, Previtali G, Seghezzi M, et al. Liver histopathology in severe COVID 19 respiratory failure is suggestive of vascular alterations. *Liver Int.* 2020;40:2110-2116.
16. Lagana SM, Kudose S, Iuga AC, et al. Hepatic pathology in patients dying of COVID-19: a series of 40 cases including clinical, histologic, and virologic data. *Mod Pathol.* 2020;33:2147-2155.
17. Heinz N, Griesemer A, Kinney J, et al. A case of an infant with SARS-CoV-2 hepatitis early after liver transplantation. *Pediatr Transplant.* 2020;24:e13778.
18. Lagana SM, De Michele S, Lee MJ, et al. COVID-19 associated hepatitis complicating recent living donor liver transplantation [published online April 17, 2020]. *Arch Pathol Lab Med.*
19. Varga Z, Flammer AJ, Steiger P, et al. Endothelial cell infection and endotheliitis in COVID-19. *Lancet.* 2020;395:1417-1418.
20. Zhao CL, Rapkiewicz A, Maghsoodi-Deerwester M, et al. Pathological findings in the postmortem liver of COVID-19 patients. *Hum Pathol.* 2021;109:59-68.
21. Foschini Mp, Sarti F, Dina RE, et al. Standardized reporting of histological diagnoses for non-neoplastic liver conditions in needle biopsies. *Virchows Arch.* 1995;426:593-596.
22. US Food and Drug Administration. CDC 2019-novel coronavirus (2019-nCoV) real-time RT-PCR diagnostic panel. 2020. https://www.fda.gov/media/134922/download. Accessed November 4, 2020.
23. Centers for Disease Control and Prevention. Research use only 2019-novel coronavirus (2019-nCoV) real-time RT-PCR primers and probes. 2020. https://www.cdc.gov/coronavirus/2019-ncov/lab/rt-pcr-panel-primer-probes.html. Accessed June 9, 2020.
24. Krafft AE, Duncan BW, Bijwaard KE, et al. Optimization of the isolation and amplification of RNA from formalin-fixed, paraffin-embedded tissue: the Armed Forces Institute of Pathology experience and literature review. *Mol Diagn.* 1997;2:217-230.
25. Schaller T, Hirschbühl K, Burkhardt K, et al. Postmortem examination of patients with COVID-19. *JAMA.* 2020;323:2518-2520.
26. Martines RB, Ritter JM, Matkovic E, et al; COVID-19 Pathology Working Group. Pathology and pathogenesis of SARS-CoV-2 associated with fatal coronavirus disease, United States. *Emerg Infect Dis.* 2020;26:2005-2015.
27. Baiocchini A, Del Nonno F, Taibi C, et al. Liver sinusoidal endothelial cells (LSECs) modifications in patients with chronic hepatitis C [published online June 19, 2020]. *Sci Rep.*

DOI: 10.1093/ajcp/aqab009